Theoretical Investigation of Benzene Alkylation with Ethene over H-ZSM-5

ARTICLE *in* THE JOURNAL OF PHYSICAL CHEMISTRY C · OCTOBER 2008

Impact Factor: 4.77 · DOI: 10.1021/jp8036022

4 AUTHORS, INCLUDING:

Niels Hansen
ETH Zurich
24 PUBLICATIONS **460** CITATIONS
SEE PROFILE

Frerich J Keil
Technische Universität Hamburg-Harburg
204 PUBLICATIONS **4,839** CITATIONS
SEE PROFILE

Theoretical Investigation of Benzene Alkylation with Ethene over H-ZSM-5

Niels Hansen,*,† Till Brüggemann,† Alexis T. Bell,*,‡ and Frerich J. Keil†

Department of Chemical Engineering, Hamburg University of Technology, D-21073 Hamburg, Germany, and Department of Chemical Engineering, University of California, Berkeley, California 94720-1462

Received: April 24, 2008; Revised Manuscript Received: July 15, 2008

Benzene alkylation with ethene over zeolite H-ZSM-5 has been investigated using density functional theory. Three different reaction mechanisms—two one-step schemes and one two-step scheme—have been studied on three cluster models of increasing size representing parts of the H-ZSM-5 framework. In the one-step schemes ethene protonation and C−C bond formation occur simultaneously. The two-step scheme starts with the formation of a stable ethoxide intermediate which subsequently reacts with benzene to form the reaction product. Activation energies obtained from the DFT results have been improved by single-point MP2 calculations. The calculated intrinsic activation energies of the one-step schemes are similar to the activation energy of the alkylation step in the two-step scheme. Numerical values of the MP2 corrected activation energies are in good agreement with experimental data. The largest cluster (33 T-atoms) was found to stabilize protonated ethylbenzene as a stable intermediate. The results of this study show the importance of using relatively large clusters for investigations of hydrocarbon transformation occurring in zeolites.

Introduction

Ethylbenzene is used primarily as an intermediate in the production of styrene,[1] as well as a paint solvent and an intermediate in the pharmaceutical industry,[2] and is produced at the worldwide level of $\sim 22 \times 10^6$ t per year.[3] Most of this production is by the alkylation of benzene by ethene catalyzed by metal chloride-based liquid catalysts such as $AlCl_3$ and BF_3 that are corrosive and difficult to dispose.[4,5] The use of zeolite catalysts offers an environmentally friendly route to ethylbenzene and the possibility of achieving superior product selectivity through pore size control.[6−9] ZSM-5, a medium pore zeolite, is particularly well suited for the gas-phase alkylation of aromatics and has been used in the Mobil/Badger process since 1980.[10−12] Morevover, ZSM-5 shows a higher resistance to coking compared to cage-type zeolites like faujasite.[6,7,13]

The mechanism by which zeolites catalyze the alkylation of arenes has been investigated experimentally and found to depend on the structure of the zeolite. Smirniotis and Ruckenstein have reported that the alkylation of bulky aromatics with relatively large alkylating agents over small or medium pore zeolites occurs via a Langmuir−Hinshelwood (LH) mechanism, while the alkylation of relatively small aromatics over large pore zeolites follows the Rideal−Eley (RE) mechanism.[14] It must be recognized, however, that in the case of zeolite catalysts it is not possible to assume that any of the reactants are truly in the gas phase because they are all subjected to electric field gradients and confinement effects once inside the zeolite pores.[7] In fact, different experimental studies have concluded that the mechanism of benzene ethylation catalyzed by H-ZSM-5 is best described by a LH mechanism, in which the initial step is the coadsorption of the reactants at the acid site.[14,15]

Neutron, Raman and X-ray diffraction measurements as well as Monte Carlo simulations show that the channel intersections are the preferred sites for benzene adsorption for loadings up to 4 molecules per unit cell.[16−20] Since the pore size of H-ZSM-5 closely matches the dimensions of the reaction product, ethylbenzene, it can be assumed that the formation of this product occurs preferentially on acid sites located in the channel intersections. Mechanistic studies of benzene alkylation on different zeolites suggest that the olefin and benzene do not compete for adsorption on the acid site. The olefin is assumed to interact with the Brønsted acid site, while benzene adsorbs edge-on next to the adsorbed olefin.[21] The protonated olefin then reacts with the more weakly adsorbed benzene to form alkylbenzene. However, mechanistic details involved in going from the reactants to the final products are not well understood.

There have been relatively few theoretical studies of benzene ethylation over zeolites. Vos et al. have estimated the activation energy for this process using a fully relaxed T4 cluster.[22] The same cluster model has also been used by Arstadt et al.[23] In both studies it was assumed that ethene adsorbs on the Brønsted acid site while benzene adsorbs edge-on next to the previously adsorbed ethene. While these studies find slightly different structures for the adsorbed and transition state complexes, and as a consequence slightly different activation energies, both studies conclude that ethylbenzene is formed in one, concerted step. Since the clusters used to represent the active site are small, they do not account for electrostatic interactions of the walls with the ionic transition-state structure. A more realistic representation of the zeolite has been used by Namuangruk et al.[24] These authors employed the ONIOM3 method[25] on a 84T cluster representation of two supercages of faujasite in order to calculate the structures of the adsorbed state and the transition state. Two reaction mechanisms were considered, a two-step reaction involving the formation of a covalently bonded ethoxide intermediate via a carbenium ion-like transition state in the first step and a one-step mechanism in which protonated ethene reacts directly with benzene. The activation energy for the one-step mechanism was 5 kcal/mol lower than that for the reaction step in the two-step mechanism. Nevertheless, it was suggested that the two-step mechanism could contribute significantly to the overall rate of benzene alkylation because ethoxide formation

* To whom correspondence should be addressed. E-mail: n.hansen@tu-harburg.de (N.H.); bell@cchem.berkeley.edu (A.T.B.).
† Hamburg University of Technology.
‡ University of California, Berkeley.

10.1021/jp8036022 CCC: $40.75
Published on Web 09/10/2008

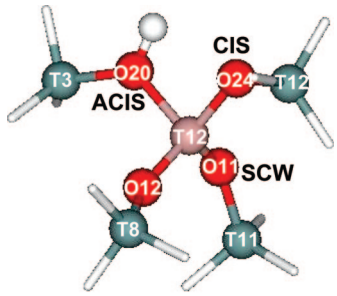

Figure 1. T5 cluster model of the acid site in H-ZSM-5. The atoms are labeled according to the crystallographic position numbers given by Olson et al.[29] Depending on its position, the bridging hydroxyl group is referred to as ACIS-, CIS, or SCW-site, respectively.

is favored kinetically. The calculated adsorption energies were found to agree well with experimental data. It should be noted, though, that this agreement is to some extent a consequence of the choice of the ONIOM approach. For example, an ONIOM2-(B3LYP/6-31G(d,p):HF/3-21G) representation overpredicts the adsorption energy of ethene[26] and considerably under-predicts the adsorption energy of benzene.[27] On the other hand, an ONIOM2(B3LYP/6-311++G(d,p):UFF) representation[28] and an ONIOM3(MP2/6-311++G(d,p):HF/6-31G(d):UFF) representation[24] provide very good agreement with the experimental adsorption energies for both ethene and benzene.

The aim of the present study is to elucidate the mechanism of benzene ethylation occurring in H-ZSM-5 using density functional theory (DFT). DFT calculations were carried out on three cluster models of progressively larger size. The size of the cluster used was found to have a significant effect on the reaction energetics and kinetics. It was also concluded that a large cluster size is required in order to capture all of the mechanistic details.

Theory

The catalytically active center and a portion of the zeolite framework were represented by clusters containing 5, 17, and 33 T-sites, respectively. Initially all Si atoms were placed at their crystallographic positions, as reported by Olson et al.[29] The location of Al in the zeolite framework is difficult to define. Both experimental[30−33] and theoretical[32,34,35] studies aimed at determining the preferential locations for Al substitution into ZSM-5 do not lead to a definitive conclusion because the differences in the energies associated with replacement of a Si by Al at different T sites are small. Thus, the location of Al atoms in the zeolite framework is controlled more by the kinetics of zeolite synthesis than by thermodynamics. Nevertheless, there is some evidence that Al siting is not random and that the T12 site is preferred.[30,34] Based on these findings and other theoretical studies on H-ZSM-5,[36−38] Al was located at the T12 position (see Figure 1). Terminal Si−O bonds were replaced by Si−H bonds oriented in the direction of the former Si−O bond. The Si−H bond length was set to 1.487 Å, which is the optimized bond length for SiH_4 at the B3LYP/TZVP level of theory. For the T5 cluster, the resulting coordinates for the terminal H atoms along with the coordinates for the Si atoms were held fixed throughout all subsequent calculations. For the T17 and T33 clusters (see Figures 2 and 3) only the terminal H atoms were held fixed while all other coordinates were allowed to relax. Based on the crystallographic position numbers used by Olson et al.[29] for an orthorhombic unit cell, the bridging hydroxyl group is either Al12−O24(H)−Si12, Si3−O20(H)−Al12, or Si11−O11(H)−Al12. In accordance with the literature,[36] the

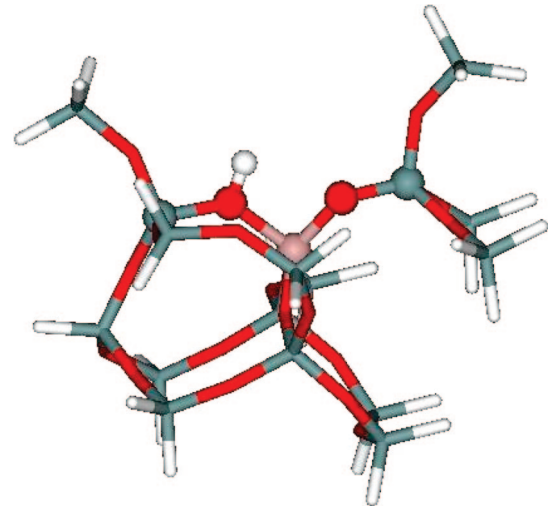

Figure 2. T17 cluster model of the active site for benzene alkylation viewed along the sinusoidal channel. The bridging hydroxyl group is in the ACIS position.

first site is called the "channel intersection" position (CIS) and the second site is called the "alternative channel intersection" position (ACIS). Since the O11 atom can be regarded as part of the straight channel wall, we refer to the third site as the "straight channel wall" position (SCW).

Quantum chemical calculations were performed with the TURBOMOLE suite of programs[39] in C1 symmetry, using gradient-corrected density-functional theory (DFT). Becke's three-parameter exchange functional[40] and the correlation functional of Lee, Yang and Parr were used to represent the effects of exchange and correlation (B3LYP).[41] The default numerical grid size (m3) was used.[42] Although it is well-known that DFT does not properly account for dispersive interactions,[43] hybrid DFT methods have proven to be very useful for elucidating the mechanism of reactions involving hydrocarbon transformation in zeolites.[38,44−49] In order to make calculations feasible for the large T33 cluster and to allow for comparisons with earlier cluster calculations,[22,23] basis sets at the double-ζ level with polarization functions (SV(P))[50] were used for all atoms. During the structure optimizations, energies were converged to 10^{-6} Ha and the maximum norm of the Cartesian gradient was converged to 10^{-3} Ha/bohr. Transition states were localized using a combination of interpolation and local methods. For the T5-cluster the growing-string method[51] was used in mass-weighted coordinates with a maximum of 13−16 nodes. After the two ends of the growing string joined, the growing-string method was terminated and an approximate saddle point was identified. The PRFO method was employed to refine the position of the saddle point.[52] Converged transition-state structures from the T5 cluster were transferred to larger clusters and used as the initial guesses. Subsequent refinement was carried out with the modified-dimer method.[53] A gradient-norm convergence criterion of 5×10^{-4} Ha/bohr was used for the transition-state searches. To confirm that the transition states were connected to the correct energy minima, each transition state was perturbed slightly along the reaction coordinate in the reactant and product directions. The perturbed geometries were then used as starting points for energy minimization. In each case the desired energy minimum was obtained.

The error in energy barriers obtained from DFT is often too large to calculate rate constants within an accuracy of 1 order of magnitude, even if hybrid functionals are used.[54] To improve the theoretical estimate of the intrinsic activation energies we

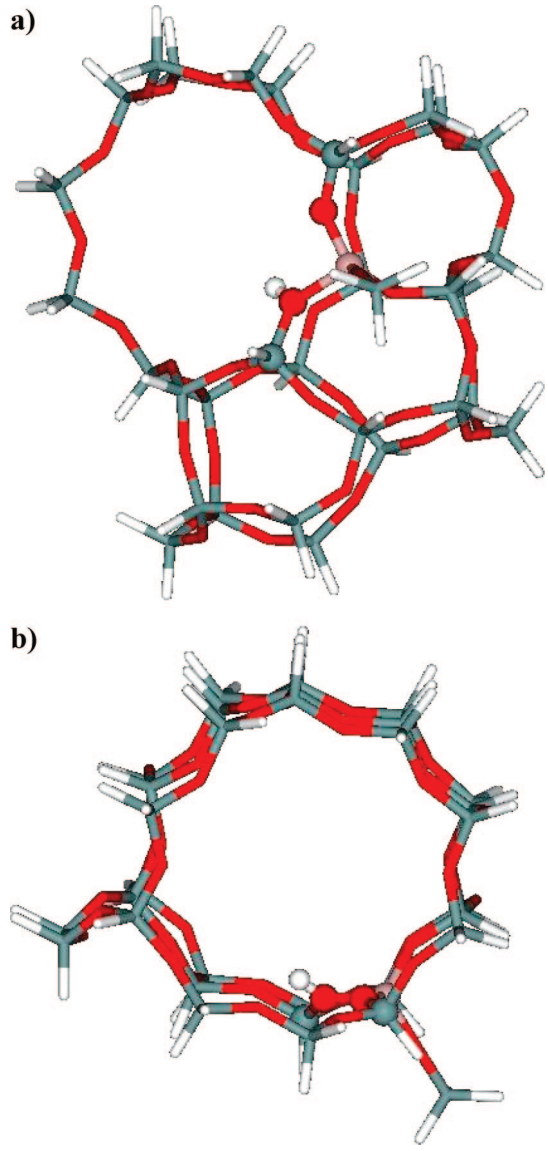

Figure 3. T33 cluster of the active site for benzene alkylation viewed along the sinusoidal channel (a) and the straight channel (b), respectively. The bridging hydroxyl group is in the ACIS position.

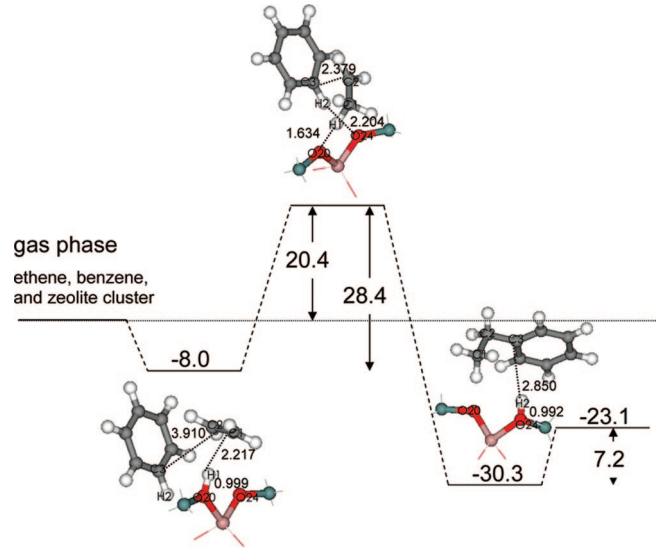

Figure 4. Energy profile (T5 cluster) for the one-step reaction involving a position change of the acidic hydrogen from the ACIS to the CIS site during the reaction. Energies are zero-point corrected. Interatomic distances are given in Å.

conducted MP2 single point energy calculations employing the quadruple-ζ basis set from Dunning's correlation-consistent polarized valence series, cc-pVXZ[55] for all atoms. We used the parallelized version of the TURBOMOLE 'ricc2′ module[56,57] and employed the resolution of the identity (RI) approximation[58−62] with optimized auxiliary basis sets[63,64] in combination with a frozen-core (FC) ansatz. Electrons in molecular orbitals corresponding to carbon 1s, oxygen 1s, aluminum 1s, and silicon 1s atomic orbitals were excluded from the MP2 correlation scheme. The use of both RI and FC approximation leads to a considerable reduction in computer time and introduces only a small error. Recent applications of this approach to zeolite catalyzed hydrocarbon reactions and proton jumps in zeolites are reported in refs 43 and 65−67. To estimate the error introduced by the FC approximation in the present study, we calculated the intrinsic activation energy for the one-step alkylation on the T5 cluster (using the DFT-converged geometries; see Figure 4) employing an all electron (AE) correlation treatment. The energy difference between the RI-MP2(AE) and RI-MP2(FC) calculation is <0.1 kcal/mol. To justify the use of DFT-converged transition state structures for single point RI-MP2(FC) calculations, we also calculated the intrinsic activation energy of the one-step alkylation for the T5 cluster by optimizing both reactant and transition state at the RI-MP2(FC)/cc-pVTZ level (the terminating SiH_3 groups were held fixed). The difference in electronic energy between the activation energy obtained from single point RI-MP2(FC) calculations on the DFT-converged structures and the optimized calculation is <0.2 kcal/mol, leading us to conclude that the use of DFT-converged structures for single point RI-MP2(FC)/cc-pVQZ calculation is a reasonable approximation for both energy minima and transition state structures. In the following all RI-MP2(FC) calculations are referred to simply as MP2 calculations.

The reason for using the T33 cluster was to account for the electrostatic stabilization of the ionic transition state structure through the framework atoms. However, single point MP2 calculations with large basis sets cannot be carried out for reasons of computational costs for the T33 cluster even if the RI and FC approximations are used. In order to improve the activation energy obtained from DFT calculations on this cluster we carved out T5 clusters similar to the one shown in Figure 1 from the DFT-converged T33 geometries of both transition state and adsorption complex and used these for single point MP2 calculations. A corrected intrinsic activation energy, $E_{a,corr}$, was then obtained from

$$E_{a,corr} = E^{DFT}_{a,T33} + \left(E^{MP2}_{a,T5\leftarrow T33} - E^{DFT}_{a,T5\leftarrow T33}\right) \quad (1)$$

where $E^{DFT}_{a,T33}$ is the activation energy obtained on the T33-cluster at the DFT level. $E^{MP2}_{a,T5\leftarrow T33}$ denotes the activation energy obtained from single point MP2 calculations on the T5 cluster cut out from the DFT optimized T33 structures. Likewise, $E^{DFT}_{a,T5\leftarrow T33}$ is the activation energy obtained from single point DFT calculations on this cluster. The term in brackets can thus be interpreted as the high level correction to the DFT activation energy calculated for the T33 cluster.

Intrinsic reaction rate constants were computed using standard statistical mechanics and absolute rate theory.[68] We used the harmonic approximation, and assumed that adsorbate and transition state are rigid in space and have only vibrational degrees of freedom.

Results and Discussion

Three reaction mechanisms were considered. Two of them are concerted schemes, which differ only in whether or not the position of the acidic hydrogen changes during the course of reaction. The third mechanism involves the formation of a stable ethoxide intermediate in the first step. In what follows we review first the energetics for each of the mechanisms obtained using the T5 cluster. Second, we illustrate the energetic and structural differences that arise using the T17 cluster. Third, we present the results for the T33 cluster and show that not only energetic and structural but also mechanistic differences are obtained. Fourth, we discuss the results of the present study in the light of previous theoretical studies and, where available, experimental data. All computed adsorption and reaction energies reported in this section are zero-point energy corrected DFT results obtained with the B3LYP functional in combination with the SV(P) basis set (see Theory section for details). Activation energies presented for the T5 and T17 cluster were also calculated at this level of theory. Both DFT and MP2-corrected activation energies are presented for the T33 cluster.

Mechanisms of Benzene Alkylation with Ethene Calculated for the T5 Cluster. Figure 4 illustrates the alkylation mechanism in which the position of the Brønsted acidic proton moves from the ACIS to the CIS site during the reaction. Initially, ethene adsorbs on the acid site while benzene adsorbs edge-on next to the active site. The O20−H1 bond is slightly elongated compared to the bare cluster (0.999 Å in the adsorbed state and 0.975 Å for the bare cluster), indicative of only weak interaction between ethene and the proton. The C1−C2 double bond length is virtually unchanged (1.335 Å in the gas phase and 1.341 Å in the adsorbed state). An adsorption energy of $\Delta E_{ads} = -8.0$ kcal/mol was calculated for the coadsorption of ethene and benzene from the gas phase. It should be noted that the opposite scenario, i.e. benzene adsorbed on the acid site and ethene coadsorbed, was also evaluated. While this configuration cannot be ruled out based on adsorption energies, a physically meaningful transition state for the formation of ethylbenzene could not be obtained in this case. Therefore, it appears that ethylbenzene is formed only when ethene interacts with the acid site. In the one-step mechanism, ethene is protonated and attacked by the adsorbed benzene to produce ethylbenzene. The activation energy for this process is $E^{\ddagger} = 28.4$ kcal/mol. In going from the reactant state to the transition state the O20−H1 distance lengthens from 0.999 to 1.634 Å. The length of the C1−C2 bond increases from 1.341 to 1.429 Å, while the distance between the bond forming C-atoms of ethene and benzene (C2−C3) decreases from 3.910 to 2.379 Å. The imaginary frequency associated with vibration along the reaction coordinate is $192i$ cm^{-1}. The desorption energy for the product ethylbenzene is $\Delta E_{des} = 7.2$ kcal/mol.

The second one-step mechanism, illustrated in Figure 5, differs from the one presented in Figure 4 in that the acidic proton remains in the same position after the reaction as it was before the reaction. Both mechanisms lead to similar adsorption energies; however, the activation energy for the mechanism shown in Figure 5 is lower by 2.3 kcal/mol. Compared to the first mechanism, the distances between bond forming and bond breaking atoms of the transition state are longer (i.e., C2−C3 and H2−O20/H2−O24). The imaginary frequency associated with vibration along the reaction coordinate is $196i$ cm^{-1}. The energy to desorb ethylbenzene is $\Delta E_{des} = 6.9$ kcal/mol.

In the two-step mechanism shown in Figure 6, ethene is first adsorbed on the acid site. As already mentioned above, the interaction of ethene with the acid site is weak. The length of the O20−H1 bond increases from 0.975 to 1.000 Å, while the length of the C1−C2 double bond remains almost unchanged compared to the gas phase (1.341 Å in the adsorbed state and 1.335 Å in the gas phase). Protonation of ethene leads to a

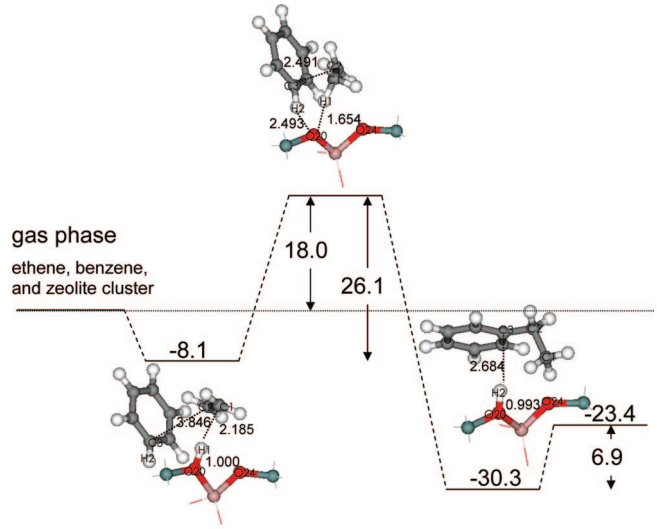

Figure 5. Energy profile (T5 cluster) for the one-step reaction in which the acidic hydrogen remains on the ACIS site during the reaction. Energies are zero-point corrected. Interatomic distances are given in Å.

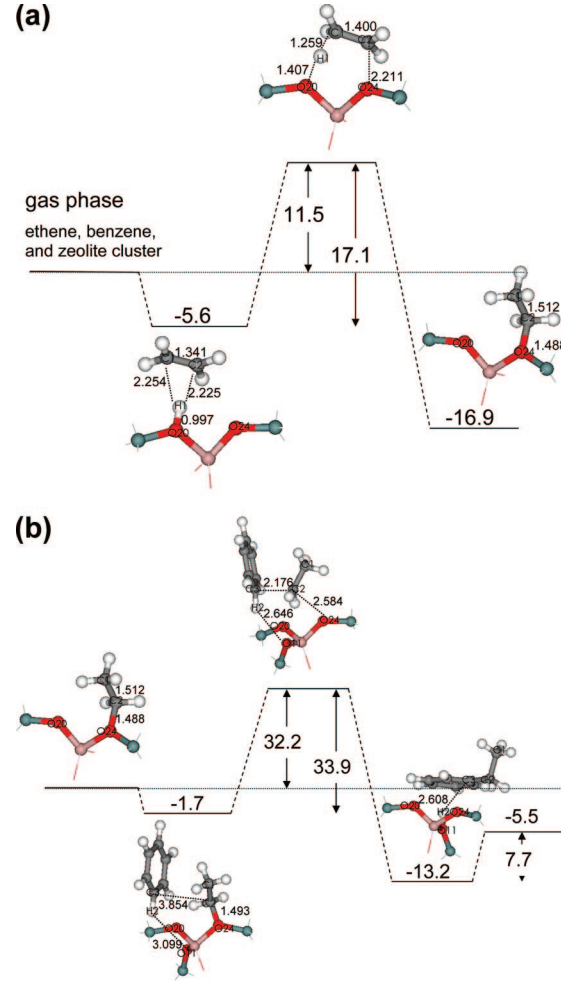

Figure 6. Energy profile (T5 cluster) for (a) the protonation of ethene to give an ethoxide species, (b) alkylation step. Energies are zero-point corrected. Interatomic distances are given in Å.

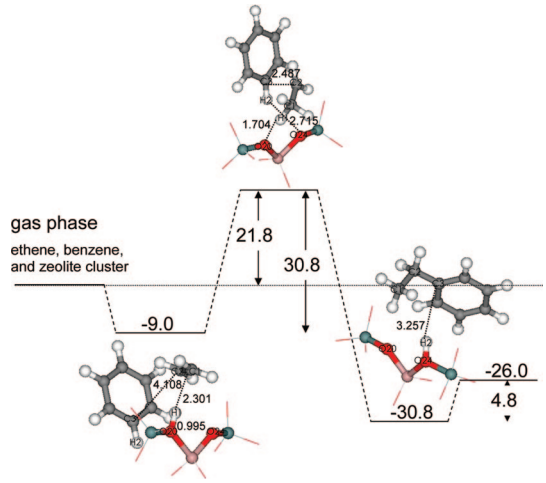

Figure 7. Energy profile (T17 cluster) for the one-step reaction involving a position change of the acidic hydrogen from the ACIS to the CIS site during the reaction. Energies are zero-point corrected. Interatomic distances are given in Å.

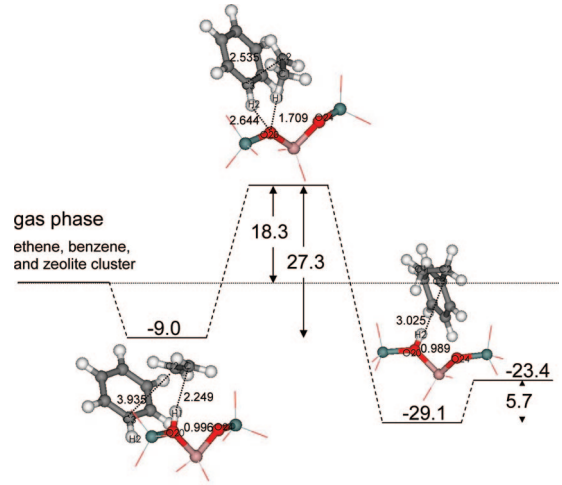

Figure 8. Energy profile (T17 cluster) for the one-step reaction in which the acidic hydrogen remains on the ACIS site during the reaction. Energies are zero-point corrected. Interatomic distances are given in Å.

covalently bonded ethoxide. The activation energy calculated for this process is $E^{\ddagger} = 17.1$ kcal/mol. In the transition state the O20−H1 bond is lengthened to 1.407 Å, while the C1−C2 bond length increases to 1.400 Å. The imaginary frequency associated with the transition mode is $469i$ cm^{-1}. The ethoxide species is more stable by 11.3 kcal/mol relative to the π-complex. Benzene interacts only weakly with the ethoxide species (Figure 6b). The activation energy calculated for the formation of ethylbenzene is $E^{\ddagger} = 33.9$ kcal/mol and, thus, is 6−8 kcal/mol higher than that for the one-step mechanisms. In the transition state the distances between the bond forming atoms (C2 and C3) are significantly shorter (2.176 Å) than those seen in the transition states of the one-step mechanisms. The imaginary frequency associated with vibration along the reaction coordinate of the transition state mode is $141i$ cm^{-1}. Note that the proton is donated to the SCW site in this case. A reaction channel resulting in proton donation to the ACIS or CIS site could not be identified.

Mechanisms of Benzene Alkylation with Ethene Calculated for the T17 Cluster. Figure 7 illustrates the first of the one-step mechanisms occurring on the T17 cluster. The adsorption energy of the coadsorbed complex is higher than that for the T5 cluster by 1 kcal/mol, reflecting the greater interaction of the adsorbates with the increased number of framework atoms. The characteristic distances between the adsorbed complex and the framework are slightly larger than those for the T5 cluster. The distance between ethene and the acid site (H1−C1) is larger by 0.1 Å, while the distance between the bond forming C atoms of benzene and ethene is larger by 0.2 Å. The activation energy for the formation of ethylbenzene is $\Delta E^{\ddagger} = 30.8$ kcal/mol which is 2.5 kcal/mol higher than that calculated for the T5 cluster. The imaginary frequency associated with vibration along the reaction coordinate is $161i$ cm^{-1}. The atomic distances O20−H1 and C2−C3 are only slightly larger than for the T5 cluster. However, the O24−H2 distance (2.715 Å) is significantly larger, showing the influence of the additional framework atoms surrounding the active site. While the T5 cluster does not represent a particular pore architecture, the additional wall atoms included in the T17 cluster cause the transition state to rotate into the free space of the channel intersection rather than remaining close to the cluster. The distance between the reaction product and the acid site is larger by 0.4 Å compared to the T5 cluster resulting in a desorption energy of only 4.8 kcal/mol.

Figure 8 illustrates the second one-step mechanism occurring for the T17 cluster. The adsorption energy of the coadsorbed complex is higher than that for the corresponding mechanism for the T5 cluster by 0.9 kcal/mol. The distance between the bond-forming C2 and C3 atoms is larger than for the case of the T5 cluster (2.535 vs 2.491 Å) as is the distance between the bond-forming H2 and O20 atoms (2.644 vs 2.493 Å). The activation energy for the formation of ethylbenzene is $E^{\ddagger} = 27.3$ kcal/mol, which is 1.2 kcal/mol higher than that calculated for the T5 cluster. The imaginary frequency associated with vibration along the reaction coordinate is $142i$ cm^{-1}. The characteristic atomic distances of the transition state (i.e O20−H1, O20−H2, and C2−C3) are all slightly longer than those for the T5 cluster. The distance between the reaction product and the acid site is larger by 0.3 Å compared to that for the T5 cluster, resulting in an adsorption energy that is lower by 5.7 kcal/mol.

The differences between the two one-step schemes for the T17 cluster are qualitatively the same as those calculated for the T5 cluster. For the second mechanism, the reactants are slightly closer to the active site in the adsorbed state, while the distance between the bond forming C-atoms (C2−C3) is larger in the transition state. The activation energy for the second mechanism is lower than that for the first one by 3.5 kcal/mol.

Figure 9a shows the formation of the ethoxide on the T17 cluster. The adsorption energy for the π-complex formation ($\Delta E_{ads} = 5.5$ kcal/mol) is very similar to that for the T5 cluster, indicating that ethene adsorption is not strongly affected by the presence of the wall atoms. However, the C1−H1 and C2−H1 distances are larger than those found for the T5 cluster. The same holds for the transition state (O20−H1 and C2−O24 distances). The activation energy is 4.1 kcal/mol higher than that for the T5 cluster. The imaginary frequency for vibration along the reaction coordinate is $352i$ cm^{-1}. The ethoxide species is stabilized by 10.1 kcal/mol relative to the π-complex. The C−O bond length of the ethoxide is virtually the same as that determined for the T5 cluster (1.488 Å on T5 and 1.493 Å on T17). Benzene interacts weakly with the ethoxide ($\Delta E_{ads} = -2.9$ kcal/mol). The activation barrier for ethylbenzene formation is $\Delta E^{\ddagger} = 39.8$ kcal/mol, about 6 kcal/mol larger than that for the T5 model. The imaginary frequency for vibration along the reaction coordinate is $128i$ cm^{-1}. As before, the proton is donated to the SCW site. The stable product state is far away

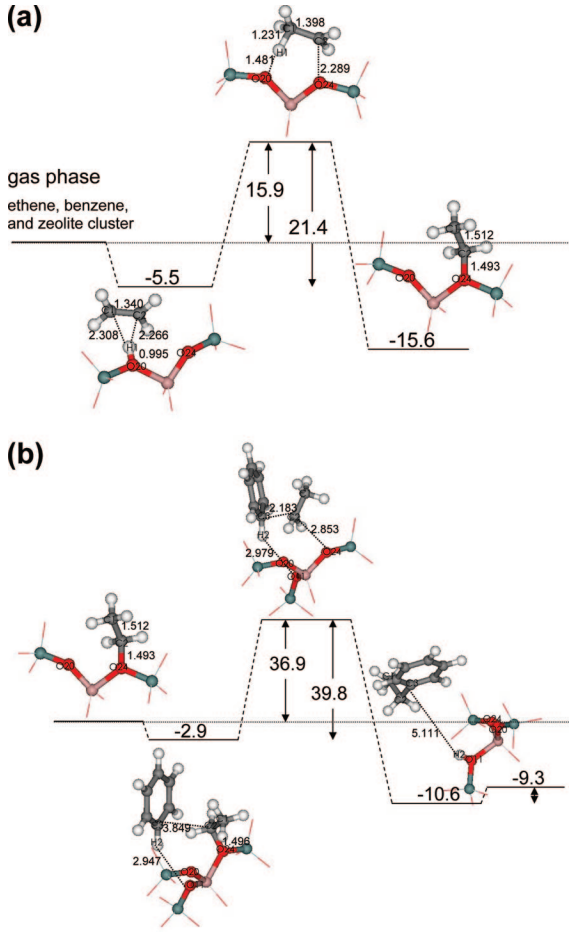

Figure 9. Energy profile (T17 cluster) for (a) the protonation of ethene to give an ethoxide species, (b) alkylation step. Energies are zero-point corrected. Interatomic distances are given in Å.

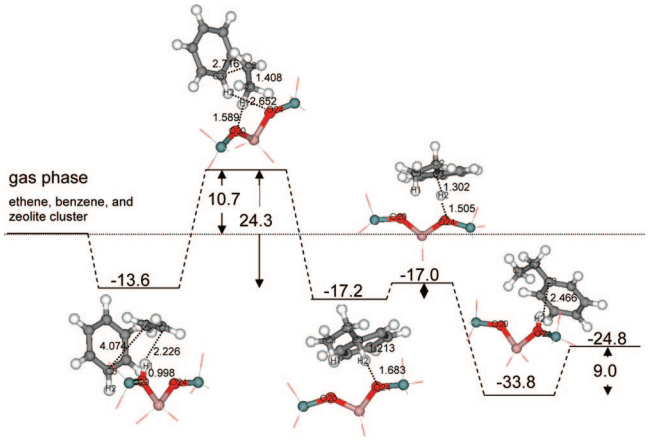

Figure 10. Energy profile (T33 cluster) for the one-step reaction involving a position change of the acidic hydrogen from the ACIS to the CIS site during the reaction. Energies are zero-point corrected. Interatomic distances are given in Å.

from the acid site due to steric constraints imposed by the walls of the straight channel. Consequently the computed desorption energy is low (ΔE_{des} = 1.3 kcal/mol).

Mechanisms of Benzene Alkylation with Ethene for the T33 Cluster. Figure 10 illustrates the alkylation mechanism in which the position of the acidic proton changes from the ACIS to CIS site. The interatomic distances between ethene and the Brønsted site (H1−C1) and between the adsorbates (C2−C3) are larger than those for the T5 cluster but not to the same extent as was the case for the T17 cluster. This reflects the effects of confinement imposed by the additional framework atoms on the opposite side of the active center. The adsorption energy was calculated to be $\Delta E_{ads} = -13.6$ kcal/mol, which is significantly larger than that determined for the smaller clusters. The activation energy for the formation of ethylbenzene is $\Delta E^{\ddagger} =$ 24.3 kcal/mol. This value is 4−6 kcal/mol lower than that calculated for the smaller clusters. The observed stabilizing effect of the zeolite micropore on the ionic transition state is well-known[37,69−71] and can be on the order of 10−30% of activation energies obtained for small clusters. In the transition state, the distance between the bond forming C-atoms (C2−C3) is larger than that obtained for the smaller clusters (T33, 2.716 Å; T17, 2.487 Å; T5, 2.379 Å). The distance between the bond breaking H1 and O20 atoms is smallest for the T33 cluster (T33, 1.589 Å; T17, 1.704 Å; T5, 1.634 Å). The distance between the bond forming O2 and H24 atoms lies between those for the smaller clusters (T33, 2.652 Å; T17, 2.715 Å; T5, 2.204 Å), indicating the effect of confinement imposed by the framework atoms on the opposite side of the active center. The imaginary frequency for vibration along the reaction coordinate is 155*i* cm^{-1}.

However, the most significant difference between the large cluster and the smaller clusters is that the large cluster is able to stabilize an ionic intermediate. While ethylbenzene was formed directly from the first transition state on the T5 and T17 clusters, a stable carbenium ion (protonated ethylbenzene) was found on the T33 cluster. The intermediate has an elongated C3−H2 bond of 1.213 Å. The C1−C2 and the C2−C3 bond lengths are 1.529 and 1.547 Å, respectively. The corresponding bond lengths of protonated ethylbenzene in the gas phase are 1.124 (C3−H2), 1.526 (C1−C2), and 1.588 Å (C2−C3). In addition to a significantly longer C3−H2 bond, the adsorbed structure also possesses a larger angle between the plane spanned by the aromatic ring atoms and the C2-atom (157.6°) compared to the gas phase (139.3°). In the transition state the C3−H2 bond length increases to 1.302 Å. The imaginary frequency for vibration along the reaction coordinate is 483*i* cm^{-1}, and the product ethylbenzene interacts only weakly with the acid site. Compared to the bare cluster, the O24−H2 distance is slightly elongated from 0.979 to 0.991 Å. The C1−C2 distance is virtually unchanged (1.539 Å in the gas phase and 1.538 Å in the adsorbed state). The same holds for the C2−C3 distance (1.516 Å in the gas phase and 1.518 Å in the adsorbed state).

A mechanism in which the proton does not change its position could not be identified, in contrast to what was found for the smaller clusters, even though two different initial reactant states both corresponding to a different transition state structure could be found. However, structure optimization from the slightly perturbed transition states toward the products lead to very similar intermediate states, i.e. protonated ethylbenzene, in which the proton (H2) points toward the CIS site in both cases.

The reaction scheme with the alternative reactant and transition states is shown in Figure 11. It exhibits the same characteristics as those for the second one-step mechanisms on the smaller clusters, i.e., smaller interatomic distances in the reactant state and a smaller activation energy. The protonated ethylbenzene has a slightly shorter C3−H2 bond length. Because of the similarities in the two protonated intermediates the calculation of the transition state for the back-donation of the proton to the zeolite framework was not pursued.

Figure 12a shows the formation of an ethoxide species on the T33 cluster. In the adsorbed π-complex, the O20−H1 bond length is 1.000 Å, while the length of the C1−C2 double bond

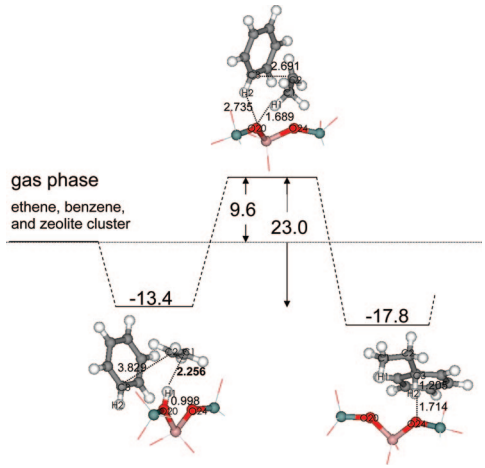

Figure 11. Energy profile (T33 cluster) for the alternative one-step reaction involving a position change of the acidic hydrogen from the ACIS to the CIS site during the reaction. Energies are zero-point corrected. Interatomic distances are given in Å.

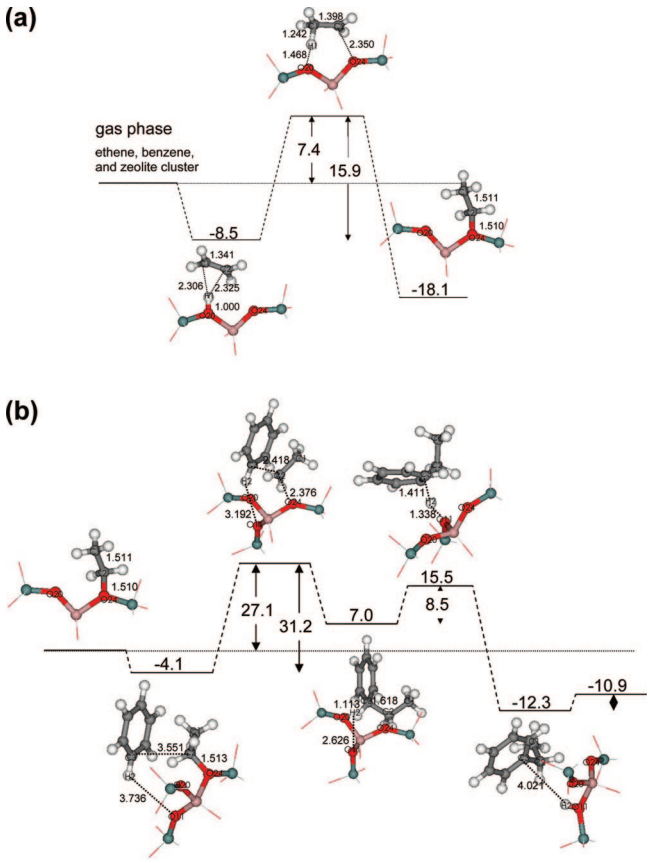

Figure 12. Energy profile (T33 cluster) for (a) the protonation of ethene to give an ethoxide species, (b) alkylation step. Energies are zero-point corrected. Interatomic distances are given in Å.

remains almost unchanged compared to that for ethene in the gas phase (1.341 Å in the adsorbed state and 1.335 Å in the gas phase). The protonation of ethene to give a covalently bonded ethoxide has an activation energy of 15.9 kcal/mol, which is only 1.2 kcal/mol lower than that for the T5 cluster. In the transition state the O20−H1 bond is lengthened to 1.468 Å, while the C1−C2 bond length increases to 1.398 Å. The imaginary frequency for vibration along the reaction coordinate is 309*i* cm^{-1}. The ethoxide intermediate is stabilized by 9.6 kcal/mol with respect to the π-complex. The CO bond length is only slightly longer than the computed distances for the smaller clusters. Benzene interacts weakly with the ethoxide ($\Delta E_{ads} = -4.1$ kcal/mol). The C2−O24 bond length is 1.513 Å and thus virtually unchanged (Figure 12b). The activation energy for the ethylbenzene formation is $\Delta E^{\ddagger} = 31.2$ kcal/mol, which is 2.7 kcal/mol smaller than the corresponding value for the T5 cluster. In the transition state the C2−O24 distance is lengthened to 2.376 Å. The distance between the reacting carbon atom of the ethene (C2) and benzene (C3) is 2.418 Å. The distance between the hydrogen atom to be back-donated to the framework and the accepting oxygen (O11) now decreases to 3.192 Å. The imaginary frequency for vibration along the reaction coordinate is 189*i* cm^{-1}. Perturbation of the transition state structure in the direction of the product and subsequent optimization, leads again to a stable carbenium like-ion. Compared to the final adsorbed ethylbenzene, the C2−C3 bond length is considerable longer in the intermediate state (1.618 Å and 1.515 Å). The activation energy for back-donation of the proton from the carbenium ion to the SCW-site of the zeolite framework is relatively large, 8.5 kcal/mol, when compared to the corresponding activation energy for the one-step mechanism. The reason is that the formation of the stable product requires extensive rearrangements in the zeolite cavity. The imaginary frequency for vibration along the reaction coordinate is 189*i* cm^{-1}. The calculated desorption energy for ethylbenzene from this site is 1.4 kcal/mol.

The stability of the ethoxide species is a critical issue for the two-step mechanism, and previous investigations have shown that the stability of alkoxide species depends strongly on the local structure of the Brønsted acid site.[72,73] For this reason, the energy of ethoxide species bonded to the ACIS site was computed, in order to estimate the influence of the nonequivalency of the framework oxygen atoms surrounding the Al-atom. In contrast to the bridging hydroxyl group, the ethoxide species is somewhat more stable on the ACIS site than on the CIS site (energy difference: 1.5 kcal/mol for T33 cluster). The cluster size also has a small influence on the stability of the ethoxide species. The zero-point energy corrected reaction energies for the ethoxide formation on the CIS site with respect to the π-complex are $\Delta E_{T5} = -11.3$ kcal/mol, $\Delta E_{T17} = -10.1$ kcal/mol, and $\Delta E_{T33} = -9.6$ kcal/mol for the T5, T17, and T33 cluster, respectively. The finding that the alkoxide species are much more stable than the corresponding adsorbed alkene is consistent with the findings of Nieminen et al.,[73] who investigated alkoxide formation in H-FER using a hybrid quantum mechanics/molecular mechanics (QM/MM) method. Contrary to these findings are the results reported by Namuangruk et al. in their study of benzene alkylation over H-FAU.[24] Here, the π-complex and the ethoxide were found to be equally stable. A possible reason for this discrepancy might be that in the latter study only a very small reactive region consisting of 3 T-atoms was allowed to relax while the surrounding framework atoms were kept fixed in their crystallographic positions.

The computed adsorption energies and enthalpies of adsorption at 300 K for ethene, benzene, ethylbenzene, and ethene coadsorbed with benzene are listed in Table 1 for all of the clusters considered in this study. Also shown for comparison are theoretically obtained values of the adsorption energies reported by Vos et al.[22] and Arstadt et al.[23] and experimental values of the adsorption enthalpy,[74−78] where these are available. Our theoretical results for ethylbenzene adsorption and ethene coadsorption with benzene obtained using the T5 cluster are very similar to the values reported by Vos et al.[22] and Arstadt et al.[23] Due to their high reactivity, the adsorption of olefins, with the exception of ethene, is difficult to study experimen-

TABLE 1: Adsorption Energies (Zero-Point Corrected) and Enthalpies (at 300 K) of Ethene (E), Benzene (B), Ethylbenzene (Eb), and Ethene Plus Benzene (E+B) on the ACIS Site and of Benzene Adsorbed in the Vicinity of the Ethoxide Intermediate for Different Cluster Sizes (in kcal/mol); Experimental Heats of Adsorption Are Given for Comparison, Where Available

		E on ACIS	B on ACIS	Eb on ACIS	E+B on ACIS	B on ethoxide
T5 (this work)	E_{ads} (ΔH_{ads})	−5.6 (−5.8)	−6.2 (−5.5)	−6.8 (−6.1)	−8.0 (−6.6)	−1.7 (−0.7)
T17 (this work)	E_{ads} (ΔH_{ads})	−5.5 (−5.2)	−5.2 (−4.5)	−5.6 (−4.9)	−9.0 (−7.9)	−2.9 (−1.3)
T33 (this work)	E_{ads} (ΔH_{ads})	−8.5 (−8.4)	−10.0 (−9.5)	−9.5 (−9.2)	−13.6 (−12.6)	−4.1 (−3.3)
T4[a] (ref 22)	E_{ads}	−	−	−6.4	−7.3	−
T4[a] (ref 23)	E_{ads}	−	−	−6.2	−7.9	−
exptl	H_{ads}	−9.0[b]	−14.3[c]	−18.0[d]	−	−
			−15.3 ± 1.2[e]	−20.7 ± 1.2[e]	−	−
			−15.2[f]			

[a] Relaxed cluster, B3LYP/6-31G*. [b] HY.[74] [c] 2 molec/uc, Si/Al = 82.[75] [d] Silicalite.[76] [e] 2 molec/uc, Si/Al = 34, but large amounts of extraframework Al.[77] [f] 1 molec/uc, Si/Al = 86.[78]

TABLE 2: Intrinsic Activation Energies in kcal/mol; Values Obtained in the Present Work Are Zero-Point Energy Corrected and Reported as DFT Results and MP2-Corrected Results (In Brackets); Values from the Literature are DFT Results and MP2/ONIOM Results (In Italics)

	concerted mechanism[a]		concerted mechanism[b]	stepwise mechanism[c]		
	TS1	TS2	TS1	TS1	TS2	TS3
T5 (this work)	28.3	N/A	26.1	17.1	33.9	N/A
T17 (this work)	30.8	N/A	27.3	21.4	39.8	N/A
T33 (this work)	24.3(28.8)	0.2	N/A	15.9(23.7)	31.2(26.4)	8.5
	23.0(25.5)	0.2				
T4[d] (ref 22)	31.5	N/A	−	−	−	−
T4[e] (ref 23)	31.3 *38.2*	N/A	−	−	−	−
T84[f] (ref 24)	*33.4*	−	−	*30.1*	*38.2*	−

[a] Brønsted H changes to CIS site during the reaction. [b] Brønsted H remains on ACIS site. [c] Brønsted H changes to SCW site during the reaction. [d] Relaxed T4-cluster, B3LYP/6-31G*. [e] First value, relaxed T4-cluster, B3LYP/6-31G*; second value, single point MP2/6-311G** on DFT-converged geometry. [f] ONIOM(MP2/6-311++G(d,p):HF/6-31G(d):UFF)//ONIOM(MP2/6-31G(d,p):HF/3-21G:UFF) applied to T84 cluster of H-FAU.

tally.[79] The interactions of ethene with Brønsted acid sites are so weak that the resulting complexes are unstable at room temperature[80] and, hence, reliable values for heats of adsorption on other than pure silica MFI zeolites are hard to obtain. The only available experimental value is that reported by Cant and Hall for ethene adsorbed on faujasite ($\Delta H_{ads} = -9$ kcal/mol).[74] However, this value can only be regarded as a lower bound because the acidity of H-ZSM-5 is known to be larger than that of faujasite.[81−85] Not surprisingly, the heats of adsorption obtained with T5 and T17 cluster are significantly lower than those observed experimentally due to the inability of such small clusters to properly account for all of the dispersive interactions of the adsorbate with the zeolite pore channels. However, when a T33 cluster is used to represent the zeolite, the difference between experimental and computed values becomes smaller.

The activation energies for benzene ethylation via all of the mechanisms considered in this study are summarized in Table 2. In each case, the calculated activation energy is higher for the T17 than for the T5 cluster, but is lowest for the T33 cluster. Since the T33 cluster includes the atoms of an entire intersection, we expect the reported activation energies not to change very much for clusters larger than T33. This is supported by a recent study on alkene methylation over H-ZSM-5, which included a systematic investigation of the dependence of the activation energy on the cluster size.[67] The calculated values of the activation energy obtained in the present study for the concerted mechanism, in which the proton moves to the CIS site during reaction, agree reasonably well with activation energies reported by Vos et al.[22] and Arstad et al.[23] for T4 and T5 clusters, respectively. MP2-corrected values of the activation energies are shown in parentheses in Table 2. With the exception of the second barrier in the two-step scheme the corrections are all positive. Table 2 shows that the MP2-corrected barriers are significantly smaller than the barriers reported by Namuangruk et al. for both the concerted and stepwise mechanisms of benzene ethylation occurring in H-FAU.[24] The reason might be that the stabilizing effect of the zeolite micropore is not so strong in the employed ONIOM approach because only a small part (12 T-atoms) of the cluster was treated quantum mechanically. This view is supported by comparing the single-point MP2 activation energies, $E^{MP2}_{a,T5\leftarrow T33}$, with the values reported by Namuangruk et al. The numbers computed in the present study are 37.5 and 35.8 kcal/mol for the two 1-step mechanisms and 28.5 and 35.9 kcal for the first and second step of the 2-step mechanism and thus similar to the barriers reported by Namuangruk et al.

TABLE 3: Rate Coefficients for Elementary Processes on the T33 Cluster Calculated with MP2-Corrected Activation Energies

		T, K		
reaction scheme	constant[a]	600	650	700
Figure *10*	k_1, s^{-1}	8.17×10^{-1}	4.97×10^{0}	2.33×10^{1}
	k_{-1}, s^{-1}	3.80×10^{-5}	9.75×10^{-4}	1.58×10^{-2}
Figure *11*	k_1, s^{-1}	2.13×10^{-1}	1.01×10^{0}	3.82×10^{0}
	k_{-1}, s^{-1}	7.23×10^{-6}	1.48×10^{-4}	1.98×10^{-3}
Figure *12*	k_1, s^{-1}	2.58×10^{2}	1.14×10^{3}	4.11×10^{3}
	k_{-1}, s^{-1}	1.20×10^{1}	1.12×10^{2}	7.65×10^{2}
	k_2, s^{-1}	3.19×10^{2}	1.84×10^{3}	8.26×10^{3}
	k_{-2}, s^{-1}	7.24×10^{-1}	6.98×10^{0}	4.87×10^{1}

[a] Rate constants for the backward reaction are determined with respect to the final product.

Rate coefficients for all reaction steps investigated in this study are listed in Table 3. The values were computed using the MP2 corrected barriers calculated for the T33 cluster, and all partition functions were evaluated with the frequencies from

the DFT calculations. For the mechanisms presented in Figures 10 and 11, it assumed that the coadsorption and desorption of ethene and benzene are quasi-equilibrated and that the rate-limiting step is the reaction of the coadsorbed reactants to form ethylbenzene. The results in Table 3 show that the rate coefficient for the scheme shown in Figure 10 is higher than that for the one shown in Figure 11. This is surprising, since the barrier for the scheme shown in Figure 11 is lower than that for the scheme shown in Figure 10. The higher value of k_1 for the scheme shown in Figure 10 is attributable to the higher value of the preexponential factor for this mechanism.

There are two critical steps in the scheme shown in Figure 12. The first is the formation of an ethoxide species via the reaction of adsorbed ethene with the Brønsted acid proton of the zeolite. This process is referred to as Reaction 1. The MP2-corrected activation barrier for this reaction is 23.7 kcal/mol (see Table 2), and the rate coefficient for this reaction, k_1, is listed in Table 3. The second critical step is the reaction of benzene adsorbed next to the ethoxide species to form ethylbenzene, Reaction 2. The MP2-corrected activation barrier for this process is 26.4 kcal/mol (see Table 2), and the rate coefficient for this reaction, k_2, is also listed in Table 3. It is evident that the rate coefficient for the reaction of ethoxide species with adsorbed benzene is significantly higher than that for the reaction of adsorbed benzene with adsorbed ethene via pathways shown in Figures 10 or 11. This relationship is surprising, since the activation barriers are similar. The reason for the higher rate coefficient for the formation of ethylbenzene via the pathway involving ethoxide species is again the higher preexponential factor for this reaction.

Table 3 shows that the two-step scheme is favored kinetically over the one-step schemes. While this could lead to the conclusion that the one-step scheme is irrelevant it should be kept in mind that the rate constant for ethoxide formation (the first step in the two-step scheme) was calculated for the case of ethene entering an empty intersection. An excess of benzene is used in industrial practice. This lowers the probability that ethene finds an unoccupied intersection, since benzene adsorbs much more strongly than ethene in the channel intersections. It is therefore likely that both mechanisms take place simultaneously. Thus, the extend to which each mechanism contributes to the overall activity is hard to establish.

Experimental activation energies for the ethylation of benzene over zeolites are rare. Christensen et al. have reported experimental values for the apparent activation energy of benzene ethylation on H-ZSM-5 of 14.1−18.4 kcal/mol.[86] whereas Becker et al. have reported an apparent activation energy over H-MOR of 10 kcal/mol.[87] To compare our calculated values to the results of Christensen et al., we assumed that the reaction proceeds via the reversible adsorption of ethene and benzene followed by the rate-limiting step in which the two coadsorbed species react to form ethylbenzene. For the case of low occupancies, the apparent activation energy, $E^{\ddagger}_{\mathrm{app}}$, is given by

$$E^{\ddagger}_{app} = E^{\ddagger} + \Delta H_{\mathrm{ads,B+E}} \qquad (2)$$

Taking values of $E^{\ddagger} = 28.8$ kcal/mol and $\Delta H_{\mathrm{ads,B+E}} = -12.6$ kcal/mol, one obtains a value of $E^{\ddagger}_{\mathrm{app}} = 16.2$ kcal/mol, in reasonable agreement with the experimentally observed values of 14.1−18.4 kcal/mol.

An important finding of the present study is the discovery that the formation of ethylbenzene involves a carbenium ion intermediate. Whether cationic species exist as true reaction intermediates or transition states within the zeolite pores, depends on charge delocalization over the cation and accessibility of the positive charge to framework oxygen atoms.[84] Both experimental[88] and theoretical studies conducted with small and large clusters[70,72] show that small carbenium ions, e.g., protonated ethene, do not occur as stable species within zeolite channels, but are present in transition states leading to the formation of alkoxide species. The conclusion about the stability of larger species, e.g., *tert*-butyl carbenium cations, depends on the choice of the computational model. Early quantum chemistry calculations employing small cluster models came to the conclusion that *tert*-butyl carbenium cations only occurred in the transition state;[89,90] however, recent periodic DFT calculations using the full zeolite unit cell have shown that *tert*-butyl carbenium cations are stable intermediates.[43] It has also been shown theoretically that cyclic carbenium ions, such as those formed during xylene disproportionation, are stable intermediates.[91,92] Experimental evidence for persistent cyclic carbenium ions in zeolites has been reported, as well.[82,93] Finally, it is noted that in the study of Namuangruk et al. on ethylbenzene formation over H-FAU, protonated ethylbenzene was not reported as stable intermediate.[24] This might be a consequence of the computational method used (only 12 out of 84 T-atoms were treated quantum mechanically) or, alternatively, of the larger pore size of FAU compared to ZSM-5 which would lead to a lower degree of cation stabilization by the zeolite walls.

Conclusions

Three reaction mechanisms for the ethylation of benzene on H-ZSM-5 have been investigated using density functional theory. Two of the mechanisms are one-step schemes, which differ only by the position of the acidic proton before and after the reaction. The third mechanism is a two-step scheme. All mechanisms have been studied on clusters of 5, 17, and 33 T atoms. Both adsorption energies as well as activation energies depend on the cluster size. The reaction barriers on the T33 cluster are significant smaller than those calculated for smaller clusters. The MP2-corrected apparent activation energies for this cluster are in good agreement with experimental data. The activation energies for the one-step schemes are slightly higher or similar to the activation energy for the alkylation step in the two-step scheme. The activation energy of the ethoxide formation is smaller than the activation energy of the one-step alkylation independent of the computational method. Since the formation of surface ethoxide species is exothermic it lowers the apparent activation energy of the two-step mechanism. In practice both the one-step and the two-step schemes are likely to contribute to the overall activity because of the significantly higher loading of benzene in the zeolite pores. In contrast to the reaction mechanisms found using small clusters, the mechanism determined for the T33 cluster involves a carbenium cation intermediate.

Acknowledgment. Computations were partly carried out at the "Norddeutscher Verbund für Hoch- und Höchstleistungsrechnen" (HLRN) on an IBM p690 Cluster. The present work was supported by the Deutsche Forschungsgemeinschaft (DFG) in priority program SPP 1155, the Fonds der chemischen Industrie, the Methane Conversion Cooperative funded by BP and the Max-Buchner Forschungsstiftung.

References and Notes

(1) Moulijn, J. A., Makkee, M., van Diepen, A. *Chemical Process Technology*; Wiley: Chichester, 2001.

(2) Degnan, T. F.; Morris Smith, C.; Venkat, C. R. *Appl. Catal., A* **2001**, *221*, 283.

(3) Hartmann, M. *Angew. Chem., Int. Ed.* **2004**, *43*, 5880.

(4) Weitkamp, J., Puppe, L., Eds. *Catalysis and Zeolites - Fundamentals and Applications*; Springer: Berlin, 1999.
(5) Perego, C.; Ingallina, P. *Catal. Today* **2002**, *73*, 3.
(6) Chen, N. Y.; Garwood, W. E. *Catal. Rev. -Sci. Eng.* **1986**, *28*, 185.
(7) Corma, A. *Chem. Rev.* **1995**, *95*, 559.
(8) Čejka, J.; Wichterlová, B. *Catal. Rev.* **2002**, *44*, 375.
(9) Corma, A. *J. Catal.* **2003**, *216*, 298.
(10) Dwyer, F. G.; Lewis, P. J.; Schneider, F. H. *Chem. Eng.* **1976**, *83*, 90.
(11) Haag, W. O., Olson, D. H., Weisz, P. B. Shape-selective catalysis in aromatics processing. In *Chemistry for the Future, Proceedings of the 29th IUPAC Congress*; Grünewald, H., Ed.; Pergamon Press: Oxford, 1984, p 327.
(12) Caeiro, G.; Carvalho, R. H.; Wang, X.; Lemos, M. A. N. D. A.; Lemos, F; Guisnet, M.; Ramôa Ribeiro, F. *J. Mol. Catal. A* **2006**, *255*, 131.
(13) Bolton, A. P. Hydrocracking, isomerization and other industrial processes, in Rabo, J. A, Ed., *Zeolite Chemistry and Catalysis*; ACS Monograph, vol. 171, American Chemical Society: Washington DC, 1976, page 714,
(14) Smirniotis, P. G.; Ruckenstein, E. *Ind. Eng. Chem. Res.* **1995**, *34*, 1517.
(15) You, H.; Long, W.; Pan, Y. *Petroleum Sci. Technol.* **2006**, *24*, 1079.
(16) Huang, Y.; Havenga, E. A. *J. Phys. Chem. B* **2000**, *104*, 5084.
(17) Goyal, R.; Fitch, A. N.; Jobic, H. *J. Phys. Chem. B* **2000**, *104*, 2878.
(18) Huang, Y.; Havenga, E. A. *Chem. Mater.* **2001**, *13*, 738.
(19) Floquet, N.; Coulomb, J. P.; Weber, G.; Bertrand, O.; Bellat, J. P. *J. Phys. Chem. B* **2003**, *107*, 685.
(20) Song, L.; Sun, Z. L.; Ban, H. Y.; Dai, M.; Rees, L. V. C. *Adsorption* **2005**, *11*, 325.
(21) Corma, A.; Martínez-Soria, V.; Schnoeveld, E. *J. Catal.* **2000**, *192*, 163.
(22) Vos, A. M.; Schoonheydt, R. A.; De Proft, F.; Geerlings, P. *J. Phys. Chem. B* **2003**, *107*, 2001.
(23) Arstad, B.; Kolboe, S.; Swang, O. *J. Phys. Chem. B* **2004**, *108*, 2300.
(24) Namuangruk, S.; Pantu, P.; Limtrakul, J. *J. Catal.* **2004**, *225*, 523.
(25) Humbel, S.; Sieber, S.; Morokuma, K. *J. Chem. Phys.* **1996**, *105*, 1959.
(26) Panjan, W.; Limtrakul, J. *J. Mol. Struct.* **2003**, *654*, 35.
(27) Raksakoon, C.; Limtrakul, J. *J. Mol. Struct.* **2003**, *631*, 147.
(28) Kasuriya, S.; Namuangruk, S.; Treesukol, P.; Tirtowidjojo, M.; Limtrakul, J. *J. Catal.* **2003**, *219*, 320.
(29) Olson, D. H.; Kokotailo, G. T.; Lawton, S. L.; Meier, W. M. *J. Phys. Chem.* **1981**, *85*, 2238.
(30) Olson, D. H.; Khosrovani, N.; Peters, A. W.; Toby, B. H. *J. Phys. Chem. B* **2000**, *104*, 4844.
(31) Dědeček, J.; Kaucký, D.; Wichterlová, B. *Chem. Commun.* **2001**, 970.
(32) Sklenak, S.; Dědeček, J.; Li, C.; Wichterlová, B.; Gábová, V.; Sierka, M; Sauer, J. *Angew. Chem., Int. Ed.* **2007**, *46*, 7286.
(33) Han, O. H.; Kim, C.-S.; Hong, S. B. *Angew. Chem., Int. Ed.* **2002**, *41*, 469.
(34) Mentzen, B. F.; Sacerdote-Peronnet, M. *Mater. Res. Bull.* **1994**, *29*, 1341.
(35) Barone, G.; Casella, G.; Giuffrida, S.; Duca, D. *J. Phys. Chem. C* **2007**, *111*, 13033.
(36) Brändle, M.; Sauer, J. *J. Am. Chem. Soc.* **1998**, *120*, 1556.
(37) Zygmunt, S. A.; Curtiss, L. A.; Zapol, P.; Iton, L. E. *J. Phys. Chem. B* **2000**, *104*, 1944.
(38) Ryder, J. A.; Chakraborty, A. K.; Bell, A. T. *J. Phys. Chem. B* **2000**, *104*, 6998.
(39) Ahlrichs, R.; Bär, M.; Häser, M.; Horn, H.; Kölmel, C. *Chem. Phys. Lett.* **1989**, *162*, 165.
(40) Becke, A. D. *Phys. Rev. A* **1988**, *38*, 3098.
(41) Lee, C.; Yang, W.; Parr, R. G. *Phys. Rev. B* **1988**, *37*, 785.
(42) Treutler, O.; Ahlrichs, R. *J. Chem. Phys.* **1995**, *102*, 346.
(43) Tuma, C.; Sauer, J. *Phys. Chem. Chem. Phys.* **2006**, *8*, 3955.
(44) Nicholas, J. B. *Top. Catal.* **1997**, *4*, 157.
(45) Frash, M. V.; Kazansky, V. B.; Rigby, A. M.; van Santen, R. A. *J. Phys. Chem. B* **1998**, *102*, 2232.
(46) Zygmunt, S. A.; Mueller, R. M.; Curtiss, L. A.; Iton, L. E. *J. Mol. Struct. (Theochem)* **1998**, *430*, 9.
(47) Furtado, E. A.; Milas, I.; Lins, J. O. M. A.; Nascimento, M. A. C. *Phys. Stat. Sol. A* **2001**, *187*, 275.
(48) Pidko, E. A.; Kazansky, V. B.; Hensen, E. J. M.; van Santen, R. A. *J. Catal.* **2006**, *240*, 73.
(49) Pereira, M. S.; Nascimento, M. A. C. *J. Phys. Chem. B* **2006**, *110*, 3231.
(50) Schäfer, A.; Horn, H.; Ahlrichs, R. *J. Chem. Phys.* **1992**, *97*, 2571.
(51) Peters, B.; Heyden, A.; Bell, A. T.; Chakraborty, A. K. *J. Chem. Phys.* **2004**, *120*, 7877.
(52) Baker, J. *J. Comput. Chem.* **1986**, *7*, 385.
(53) Heyden, A.; Bell, A. T.; Keil, F. J. *J. Chem. Phys.* **2005**, *123*, 224101.
(54) Lynch, B. J.; Truhlar, D. G. *J. Phys. Chem. A* **2001**, *105*, 2936.
(55) Dunning, T. H. *J. Chem. Phys.* **1989**, *90*, 1007.
(56) Hättig, C. *J. Chem. Phys.* **2003**, *118*, 7751.
(57) Hättig, C.; Hellweg, A.; Köhn, A. *Phys. Chem. Chem. Phys.* **2006**, *8*, 1159.
(58) Vahtras, O.; Almlöf, J.; Feyereisen, M. W. *Chem. Phys. Lett.* **1993**, *213*, 514.
(59) Whitten, J. L. *J. Chem. Phys.* **1973**, *58*, 4496.
(60) Baerends, E. J.; Ellis, D. E.; Ros, P. *Chem. Phys.* **1973**, *2*, 41.
(61) Dunlap, B. I.; Connolly, J. W. D.; Sabin, J. R. *J. Chem. Phys.* **1979**, *71*, 4993.
(62) van Alsenoy, C. *J. Comput. Chem.* **1988**, *9*, 620.
(63) Weigend, F.; Häser, M.; Patzelt, H.; Ahlrichs, R. *Chem. Phys. Lett.* **1998**, *294*, 143.
(64) Weigend, F.; Köhn, A.; Hättig, C. *J. Chem. Phys.* **2002**, *116*, 3175.
(65) Tuma, C.; Sauer, J. *Chem. Phys. Lett.* **2004**, *387*, 388.
(66) Tuma, C. A QM/QM hybrid method for MP2/plane-wave-DFT studies of extended systems. Ph.D. thesis, Humboldt-Universität zu Berlin, 2006.
(67) Svelle, S.; Tuma, C.; Rozanska, X.; Olsbye, U.; Sauer, J.; in preparation.
(68) McQuarrie, D. A. *Statistical Mechanics*; Harper Collins: New York, 1973.
(69) Milas, I.; Nascimento, M. A. C. *Chem. Phys. Lett.* **2006**, *418*, 368.
(70) Boronat, M.; Zicovich-Wilson, C. M.; Viruela, P.; Corma, A. *Chem. Eur. J.* **2001**, *7*, 1295.
(71) Sauer, J., Sierka, M., Haase, F., Acidic catalysis by zeolites: Ab initio modeling of transition structures, in Truhlar, D. G., Morokuma, K., Eds. *Transition State Modeling for Catalysis*; ACS Symp. Ser. No. 721, American Chemical Society: Washington DC, 1999, page 358.
(72) Boronat, M.; Zicovich-Wilson, C. M.; Viruela, P.; Corma, A. *J. Phys. Chem. B* **2001**, *105*, 11169.
(73) Nieminen, V.; Sierka, M.; Murzin, D. Y.; Sauer, J. *J. Catal.* **2005**, *231*, 393.
(74) Cant, N. W.; Hall, W. K. *J. Catal.* **1972**, *25*, 161.
(75) Jentys, A.; Mukti, R. R.; Tanaka, H.; Lercher, J. A. *Microporous Mesoporous Mater.* **2006**, *90*, 284.
(76) Thamm, H. *J. Phys. Chem.* **1987**, *91*, 8.
(77) Nieβen, W.; Karge, H. G.; Jozefowicz, L. *Stud. Surf. Sci. Catal.* **1993**, *80*, 475.
(78) Thamm, H.; Jerschkewitz, H.-G.; Stach, H. *Zeolites* **1988**, *8*, 151.
(79) Gorte, R. J.; White, D. *Top. Catal.* **1997**, *4*, 57.
(80) Kofke, T. J. G.; Gorte, R. J. *J. Catal.* **1989**, *115*, 233.
(81) Sarv, P.; Tuherm, T.; Lippmaa, E.; Keskinen, K.; Root, A. *J. Phys. Chem.* **1995**, *99*, 13763.
(82) Haw, J. F. *Phys. Chem. Chem. Phys.* **2002**, *4*, 5431.
(83) Simperler, A.; Bell, R. G.; Foster, M. D.; Gray, A. E.; Lewis, D. W.; Anderson, M. W. *J. Phys. Chem. B* **2004**, *108*, 7152.
(84) Xu, B.; Sievers, C.; Hong, S. B.; Prins, R.; van Bokhoven, J. A. *J. Catal.* **2006**, *244*, 163.
(85) Suzuki, K.; Noda, T.; Katada, N.; Niwa, M. *J. Catal.* **2007**, *250*, 151.
(86) Christensen, C. H.; Johannsen, K.; Schmidt, I.; Christensen, C. H. *J. Am. Chem. Soc.* **2003**, *125*, 13370.
(87) Becker, K. A.; Karge, H. G.; Streubel, W. D. *J. Catal.* **1973**, *28*, 403.
(88) Boronat, M.; Corma, A. *Appl. Catal., A* **2008**, *336*, 2.
(89) Kazansky, V. B.; Frash, M. V.; van Santen, R. A. *Appl. Catal., A* **1996**, *146*, 225.
(90) Rigby, A. M.; Kramer, G. J.; van Santen, R. A. *J. Catal.* **1997**, *170*, 1.
(91) Demuth, T.; Raybaud, P.; Lacombe, S.; Toulhoat, H. *J. Catal.* **2004**, *222*, 323.
(92) Clark, L. A.; Sierka, M.; Sauer, J. *J. Am. Chem. Soc.* **2003**, *125*, 2136.
(93) Bjørgen, M.; Bonino, F.; Kolboe, S.; Lillerud, K.-P.; Zecchina, A.; Bordiga, S. *J. Am. Chem. Soc.* **2003**, *125*, 15863.

JP8036022